JOURNAL OF SPACECRAFT AND ROCKETS
Vol. 41, No. 5, September–October 2004

Engineering Notes

ENGINEERING NOTES are short manuscripts describing new developments or important results of a preliminary nature. These Notes cannot exceed six manuscript pages and three figures; a page of text may be substituted for a figure and vice versa. After informal review by the editors, they may be published within a few months of the date of receipt. Style requirements are the same as for regular contributions (*see inside back cover*).

Nozzle Scale Optimum for the Impulse Generation in a Laser Pulsejet

K. Mori,* K. Komurasaki,† and Y. Arakawa‡
University of Tokyo, Tokyo 113-8656, Japan

Introduction

A LASER pulsejet is one of the airbreathing laser thrusters driven by repetitive laser pulses.[1] Impulsive thrust is generated by a laser-induced explosion in a divergent nozzle. Its engine cycle consists of four stages: 1) laser absorption, 2) blast-wave expansion in the nozzle, 3) exhaust, and 4) refill.

At the laser absorption stage, plasma is produced in the vicinity of beam focus. It absorbs the laser pulse energy E_i and expands quickly to drive a blast wave in a surrounding air. This stage can be characterized by the blast-wave energy efficiency $\eta_{\mathrm{bw}}(\equiv E_{\mathrm{bw}}/E_i)$. Here, the blast-wave energy E_{bw} is defined as the sum of kinetic and translational energy within the blast wave and is conserved throughout the blast-wave expansion processes in the nozzle. In our previous study, η_{bw} was extracted experimentally through the imaging of shock-wave expansion.[2] The results are summarized in Table 1.

E_{bw} is transformed to impulsive thrust in the blast wave expansion stage. Ageev et al. studied the influence of nozzle geometry on impulse using conical and parabolic nozzles and found an optimum nozzle length for certain E_i (Ref. 3). Myrabo et al. found optimum E_i for a certain nozzle geometry.[4] However, to have a general scaling law, the blast-wave expansion stage must be discussed separately from the laser absorption stage.

This study investigates the aerodynamic transformation from the blast wave to the impulsive thrust in a nozzle. An impulse imparted to a conical nozzle was measured as a function of nozzle scale, and the optimum condition was discussed, and the laser absorption stage has been characterized by measured η_{bw} listed in Table 1.

Impulse Measurement

The experimental arrangement is shown schematically in Fig. 1. A transversely excited atmospheric CO_2 pulse laser was used. The pulse duration was approximately 3 μs, in which 95% of E_i has been irradiated. Variation of E_i was less than $\pm 5\%$ pulse to pulse. An off-axial parabolic mirror was used to focus the laser beam. The f number of the focusing optics was 3.3. The laser pulse shape and the air conditions are identical to those in our previous studies.[2,5] With this optics, η_{bw} was expected at 0.44 ± 0.1 throughout the experiment. The focus of optics was set in the vicinity of the cone apex, although the impulse was not sensitive to the distance between the cone-apex and the optical focus as far as the distance was shorter than 20% of the nozzle length. The inner wall of the cone was made of aluminum, and each cone was encased in a cylinder, which was long enough to prevent a diffracted blast wave from impinging on the outer surface of the cone. Impulse I imparted to the cone was determined by the ballistic pendulum method. The pendulum displacement was measured using a laser distance measurement sensor (Keyence Inc., LK-500). Calibration was performed using an impulse hammer.[4,6] A calibration line is shown in Fig. 2. Good linearity has been obtained. Test conditions are summarized here: input energy E_i, 6–11 J; nozzle length r_n, 25–73 mm; and half-cone angle α, 15 and 30 deg.

Measured momentum-coupling coefficient $C_m(\equiv I/E_i)$ is plotted as a function of nozzle length in Fig. 3. The nozzle length r_n has

Table 1 Blast-wave energy conversion efficiency

f number	E_i, J	η_{bw}
2.2	4–11	0.47 ± 0.05
3.3	6–11	0.44 ± 0.1

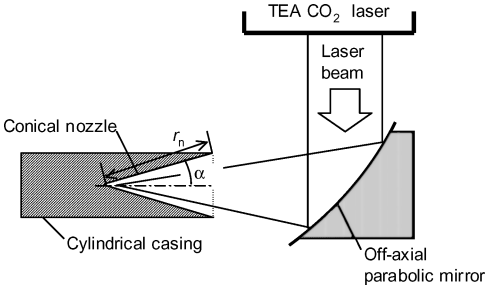

Fig. 1 Experimental arrangement.

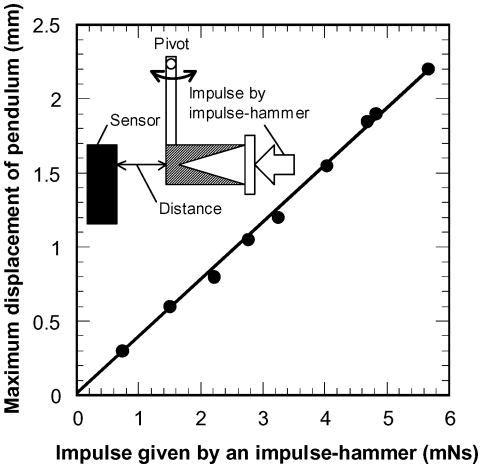

Fig. 2 Calibration line.

Received 8 October 2003; revision received 5 March 2004; accepted for publication 21 May 2004.

*Graduate Student, Department of Advanced Energy. Student Member AIAA.
†Associate Professor, Department of Advanced Energy. Member AIAA.
‡Professor, Department of Aeronautics and Astronautics. Member AIAA.

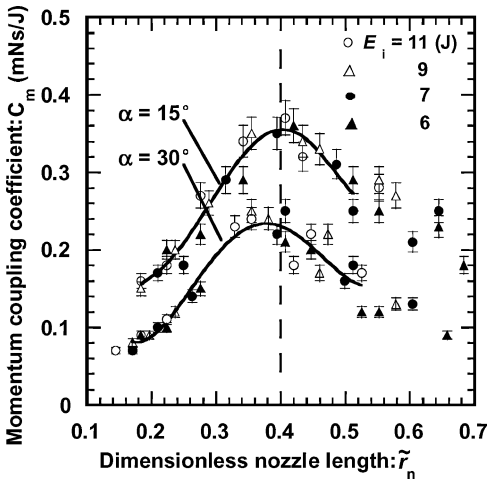

Fig. 3 Measured momentum coupling coefficient C_m and nozzle length.

been normalized by a characteristic shock-wave radius r^* defined as

$$r^* \equiv \{2E_{\rm bw}/p_a(1-\cos\alpha)\}^{\frac{1}{3}} = \{2\eta_{\rm bw}E_i/p_a(1-\cos\alpha)\}^{\frac{1}{3}} \quad (1)$$

where p_a is the ambient pressure and r^* is a function of $\eta_{\rm bw}$ and measured $\eta_{\rm bw}$ has been used here. As seen in the figure, measured C_m aligned on a unique curve of the blast-wave parameter $\tilde{r}_n$ in spite of the difference in E_i. This result suggests that C_m should be determined by the aerodynamic blast wave expansion in the nozzle. In addition, C_m has a peak at $\tilde{r}_n \sim 0.4$ for both $\alpha = 15$ and 30 deg.

Theoretical Prediction

To interpret the experimental results, the standard Sedov–Taylor solution was used because it provides analytical expressions of the shock-wave radius and the postshock pressure profiles. Although the ambient pressure is ignored in the solution, the solution will give a reasonable estimation because $E_{\rm bw}$ is conserved throughout the expansion processes. Impulse I can be calculated as an integral of time-varying thrust;

$$I = \int_0^{t_{\rm arr}} \int_0^{r_s} (p - p_a)(2\pi r \sin^2\alpha)\, {\rm d}r\, {\rm d}t \quad (2)$$

where p is the pressure, r is the radius in polar coordinates whose origin is set at the cone-apex, r_s is the location of the shock wave, subscript a represents the ambient condition, t is the elapsed time from plasma ignition, and $t_{\rm arr}$ is the time when the shock wave arrives at the exit of the cone. Here, the shifts of the explosion center caused by the laser absorption wave propagation,[5] the laser heating for finite duration, and the transition from the laser absorption wave to the aerodynamic blast wave[7–9] are ignored. In addition, the contributions of exhaust and refill stages are also ignored. Equation (2) can be transformed to

$$I = C_1 \int_0^{t_{\rm arr}} \left(\pi p_s r_s^2 \sin^2\alpha\right) {\rm d}t - p_a \int_0^{t_{\rm arr}} \left(\pi r_s^2 \sin^2\alpha\right) {\rm d}t \quad (3)$$

where

$$C_1 \equiv \int_0^1 p/p_s\, {\rm d}(r/r_s)^2$$

Here, p_s is the postshock pressure. According to the Sedov–Taylor solution of the point explosion (see Ref. 10), p/p_s is determined uniquely by r/r_s, and C_1 is a function of only the specific heat ratio γ. C_1 is 0.44 in the standard air ($\gamma = 1.4$), and r_s and p_s are also given by the Sedov–Taylor solution as

$$r_s(t) = \left(C_2 r^{*3} c_a^2 t^2\right)^{\frac{1}{5}} \quad (4)$$

$$p_s = \frac{2\rho_a}{\gamma+1}\left(\frac{{\rm d}r_s}{{\rm d}t}\right)^2 \quad (5)$$

respectively. Here, c and ρ are the sound speed and the air density, respectively, and subscript a represents the ambient condition. C_2 is a function of only γ, and its value is 0.83 for $\gamma = 1.4$ (Ref. 10).

Substituting Eqs. (4) and (5) into Eq. (3), the theoretical momentum coupling coefficient $C_{m,{\rm th}}$ is expressed as

$$C_{m,{\rm th}}(\alpha, \tilde{r}_n) = \frac{5\pi\eta_{\rm bw}(1+\cos\alpha)}{c_a\sqrt{C_2}}\left[\frac{8\gamma C_1 C_2}{25(\gamma+1)}\frac{2}{3}\tilde{r}_n^{\frac{3}{2}} - \frac{2}{9}\tilde{r}_n^{\frac{9}{2}}\right] \quad (6)$$

From the derivative of this equation, the optimum condition is deduced as

$$\tilde{r}_{n,{\rm opt}} = \left[\frac{8\gamma C_1 C_2}{25(\gamma+1)}\right]^{\frac{1}{3}} = 0.41 \quad (7)$$

This value is an invariant for the gas with $\gamma = 1.4$ and is very close to the experimental results. This good coincidence suggests that the optimum expansion condition is predictable from the balance between $E_{\rm bw}$ and the nozzle volume, and it is not so sensitive to the initial explosion processes such as the shifts of the explosion center, the laser heating for finite duration, and the transition from the laser absorption wave to the adiabatic blast wave.

Scaling Law for the Optimum Nozzle Length

Consider the example of the average laser power $\bar{P} \equiv E_i f_r$ at 100 MW, with which a vehicle of 100 kg can be launched.[11] Here, f_r is the pulse repetition frequency. Substituting Eq. (1) into Eq. (7), the optimum nozzle length $r_{n,{\rm opt}}$ can be formulated as

$$r_{n,{\rm opt}} = 0.41\left[2\eta_{\rm bw}\bar{P}/f_r p_a(1-\cos\alpha)\right]^{\frac{1}{3}} \quad (8)$$

For example, if $\eta_{\rm bw}$ can be kept at 0.44, the optimum nozzle length is calculated at 5.6 m for $f_r = 10$ Hz, and at 2.6 m for $f_r = 100$ Hz at sea level in the case of $\alpha = 15$ deg.

Conclusions

Optimum nozzle scale was formulated as $\tilde{r}_{n,{\rm opt}} = 0.41$ through the experimental and analytical studies. This scaling law would be valid for all of the gases with $\gamma = 1.4$ and independent of the effectiveness of laser absorption stage.

References

[1]Pirri, A. N., Monsler, M. J., and Nebolsine, P. E., "Propulsion by Absorption of Laser Radiation," *AIAA Journal*, Vol. 12, No. 9, 1974, pp. 1254–1261.

[2]Mori, K., Komurasaki, K., and Arakawa, Y., "Energy Transfer from a Laser Pulse to a Blast Wave in Reduced-Pressure Air Atmospheres," *Journal of Applied Physics*, Vol. 95, No. 11, 2004, pp. 5979–5983.

[3]Ageev, V. P., Barchukov, A. I., Bunkin, F. V., Konov, V. I., Korobeinikov, V. P., Putjatin, B. V., and Hudjakov, V. M., "Experimental and Theoretical Modeling of Laser Propulsion," *Acta Astronautica*, Vol. 7, No. 1, 1980, pp. 79–90.

[4]Myrabo, L. N., Libeau, M. A., Meloney, E. D., Bracken, R. L., and Knowles, T. B., "Pulsed Laser Propulsion Performance of 11-cm Parabolic 'Bell' Engines Within the Atmosphere," AIAA Paper 2002-3783, May 2002.

[5]Mori, K., Komurasaki, K., and Arakawa, Y., "Influence of the Focusing f Number on the Heating Regime Transition in Laser Absorption Waves," *Journal of Applied Physics*, Vol. 92, No. 10, 2002, pp. 5663–5667.

[6]Nakagawa, T., Mihara, Y., Komurasaki, K., Takahashi, K., Sakamoto, K., and Imai, T., "Propulsive Impulse Measurement of a Microwave-Boosted Vehicle in the Atmosphere," *Journal of Spacecraft and Rockets*, Vol. 41, No. 1, 2004, pp. 151–153.

[7]Pirri, A. N., "Theory for Momentum Transfer to a Surface with a High Power Laser," *Physics of Fluids*, Vol. 16, No. 9, 1973, pp. 1435–1440.

[8]Reilly, J. P., Ballantyne, A., and Woodroffe, J. A., "Modeling of Momentum Transfer to a Surface by Laser Supported Absorption Waves," *AIAA Journal*, Vol. 17, No. 10, 1979, pp. 1098–1105.

[9]Simons, G. A., "Momentum Transfer to a Surface When Irradiated by a High-Power Laser," *AIAA Journal*, Vol. 22, No. 3, 1984, pp. 1275–1280.

[10]Sedov, L. I., *Similarity and Dimensional Methods in Mechanics*, Academic Press, New York, 1959.

[11]Katsurayama, H., Komurasaki, K., Momozawa, A., and Arakawa, Y., "Numerical and Engine Cycle Analyses of a Pulse Laser Ramjet Vehicle," *Transaction of JSASS Space Technology*, Vol. 1, No. 1, 2003, pp. 9–16.

N. Gatsonis
Associate Editor

Prolonged Payload Rendezvous Using a Tether Actuator Mass

Paul Williams* and Chris Blanksby†
Royal Melbourne Institute of Technology, Bundoora, Victoria 3083, Australia

Nomenclature

L = tether reference length, km
l = tether length, km
m_1 = actuator mass, kg
m_2 = tether tip mass, kg
N = degree of Lagrange polynomial
R = orbit radius, km
T = tether tension, N
u = nondimensional control tension
θ = in-plane tether libration angle, rad
Λ = nondimensional tether length, l/L
ν_p = angle of payload relative to rendezvous position, rad
ν_s = angle of mother satellite relative to rendezvous position, rad
Π = actuator mass ratio, m_1/m_2
ω = orbital angular velocity of mother satellite, rad/s

Subscripts

p = payload
s = mother satellite
1 = actuator mass
2 = tether tip

Superscripts

$\cdot$ = differentiation with respect to time, $\mathrm{d}(\,)/\mathrm{d}t$
$'$ = differentiation with respect to nondimensional time, $\mathrm{d}(\,)/\mathrm{d}(\omega t)$

Introduction

SPACE tethers have been proposed for a wide range of useful applications.[1] Some of the most promising applications of tether technology involve momentum-exchange techniques. The extreme length of tethered space structures combined with the high strength and low mass of tether materials makes momentum-exchange technology a very efficient means of space transportation. Previous research has demonstrated that significant mass savings can be achieved by utilizing tether technology compared to conventional propellant systems.[2,3] Some of the more exciting momentum-exchange applications include transfer from low Earth orbit (LEO) to destinations such as the moon or Mars. Such exciting applications have been examined in some detail in Refs. 4 and 5. Other promising applications include the capture and subsequent deorbit of inoperational satellites or other space debris.[6]

Tether-mediated rendezvous has been studied previously by Stuart,[7] as well as Blanksby and Trivailo[8] for the in-plane case. Unlike traditional spacecraft rendezvous, tether-mediated rendezvous means that the target payload and mother satellite are in different orbits. Thus there might be a very short rendezvous window during which the payload and capture device are in close proximity, making capture extremely difficult.

Blanksby et al.[9] have obtained minimum reel-rate rendezvous trajectories including the case in which the orbits of all masses are not coplanar. It is probably not practical to achieve instantaneous rendezvous using current technology, as is typically required in tethered momentum transfer applications. Stuart[7] has considered this problem and proposed releasing the tether tension when the tip of the tether matches the position and velocity of the payload, thereby allowing the tether tip to more or less follow the target orbit. Corrections could be achieved using thrusters at the tether tip. However, from a practical viewpoint this is not a very desirable solution because 1) it requires propellant to be replenished at the subsatellite, 2) firing thrusters during proximity with the payload could endanger the payload, and 3) recovering control of the tether from zero or near zero tension could prove difficult. In an effort to circumvent some of these difficulties, Blanksby and Trivailo[8] considered using an additional mass that crawls along the tether to help improve the controllability of the tether tip and to extend the rendezvous window. In their work, a predictive controller was used to control the three-mass system during the rendezvous maneuver. In this Note, we consider a similar configuration and will refer to the tether crawler as an actuator mass (AM). The rendezvous maneuver is formulated as an optimal control problem and solved using a Legendre pseudospectral method. Previously, Blanksby and Trivailo[8] considered capture only at the tether tip using such a system. However, in this Note we will consider capture at both the tether tip and the actuator mass.

Equations of Motion

The assumptions used in the derivation of the equations of motion are as follows: 1) the main spacecraft (mother satellite) is sufficiently large in mass so that center of mass of the system can be assumed to coincide with the mother satellite, 2) the mother satellite is in an unperturbed circular orbit, 3) only the in-plane motion of the system is considered, 4) the system masses are considered as points masses, and 5) the tether masses are neglected. Note that in reality the center of mass will shift as the mass distribution changes, and this in turn influences the orbital motion. This coupling is neglected here but should be included in future analysis of the concepts discussed in this Note. Although only in-plane motion is studied here, perturbations will inevitably cause out-of-plane motion in the system. It is assumed that these are controlled by an appropriate means, such as tether reeling or thrusters, prior to initiating the controller for prolonging rendezvous.

Consider the jth subsatellite of mass m_j connected to the $(j-1)$th subsatellite via the jth tether, as indicated in Fig. 1a. In this Note, m_1 refers to the AM, and m_2 refers to the tether tip, as shown in Fig. 1a. The equations of motion are defined in a rotating (x, y) coordinate system, centered at C on the mother satellite. The x axis points positively outward along the orbit radius vector, and the y axis points along the orbital direction. The equations of motion including the effect of a linearized gravity gradient can be derived via Newton's second law and written as follows:

$$\ddot{x}_j - 2\omega\dot{y}_j - 3\omega^2 x_j = \frac{\left(\sum F_x\right)_j}{m_j} \tag{1}$$

Received 27 October 2003; revision received 8 March 2004; accepted for publication 1 June 2004.

*Ph.D. Candidate, School of Aerospace, Mechanical, and Manufacturing Engineering, P.O. Box 71; tethers@hotmail.com. Student Member AIAA.

†Senior Research Fellow, School of Aerospace, Mechanical, and Manufacturing Engineering, P.O. Box 71; chris.blanksby@rmit.edu.au.